BNL-223416-2022-JAAM

Localized hydrophobicity in aqueous zinc electrolytes improves zinc metal reversibility

P. Zou, X. Yang

To be published in "Nano Letters"

September 2022

Chemistry Department

Brookhaven National Laboratory

U.S. Department of Energy

USDOE Office of Energy Efficiency and Renewable Energy (EERE), Vehicle Technologies Office (EE-3V)

DISCLAIMER

Localized hydrophobicity in aqueous zinc electrolytes improves zinc metal reversibility

Peichao Zou[1‡], Ruoqian Lin[2,5‡], Travis Pollard[3], Libing Yao[1], Enyuan Hu[2], Rui Zhang[1], Yubin He[1], Chunyang Wang[1], William C. West[5], Lu Ma[4], Oleg Borodin[3], Kang Xu[3]*, Xiao-Qing Yang[2], and Huolin L. Xin[1]**

[1]Department of Physics and Astronomy, University of California, Irvine, CA, 92697 USA.

[2]Chemistry Division, Brookhaven National Laboratory, Upton, NY, 11973 USA.

[3]Battery Science Branch, Energy Science Division, Army Research Directorate, U.S.CCDC Army Research Laboratory, Adelphi, MD, 20783 USA.

[4]National Synchrotron Light Source II, Brookhaven National Laboratory, Upton, NY, 11973 USA.

[5]Jet Propulsion Laboratory, California Institute of Technology, Pasadena, CA, 91109 USA.

*Corresponding author. Email: rulin@jpl.nasa.gov (R.L.), conrad.k.xu.civ@army.mil (K.X.), huolinx@uci.edu (H.L.X.)

‡These authors contributed equally to this work.

KEYWORDS: Aqueous electrolytes, zinc metal batteries, localized hydrophobicity, alkalinity scavenging, anion-phobic diluent.

ABSTRACT: The rechargeability of aqueous zinc metal batteries is plagued by parasitic reactions of the zinc metal anode and detrimental morphologies such as dendritic or dead zinc. To improve the zinc metal reversibility, hereby we report a new solution structure of aqueous electrolyte with hydroxyl-ions scavengers and hydrophobicity localized in solvent clusters. We show that although hydrophobicity sounds counterintuitive for an aqueous system, hydrophilic pockets may be encapsulated inside a hydrophobic outer layer and a hydrophobic anode-electrolyte interface can be generated through the addition of a cation-philic, strongly anion-phobic, and OH^--reactive diluent. The localized hydrophobicity enables less active water and less absorbed water on the Zn anode surface, which suppresses the parasitic water reductions; while the hydroxyl-ion-scavenging functionality further minimizes undesired passivation layer formation, thus leading to superior reversibility (an average Zn plating/stripping efficiency of 99.72% for 1000 cycles) and lifetime (80.6% capacity retention after 5000 cycles) of zinc batteries.

Aqueous batteries offer a tantalizing solution to circumventing the safety issues of state-of-the-art lithium-ion batteries (LIBs) exclusively based on flammable, non-aqueous electrolytes. Among those, aqueous zinc metal batteries (AZMBs) hold great promise owing to their intrinsic high safety, low cost, and high theoretical energy densities.[1, 2] However, the parasitic side reactions of zinc metal (Zn^0) with water, including hydrogen evolution reaction (HER) and local high-pH induced corrosion reactions, as well as the resultant propensity of non-planar Zn electrodeposit formation on the anode side, constitute a barrier to practical applications of AZMBs, which fail on poor anode reversibility, gassing, and electrolyte consumption. The side reactions on Zn^0 surface are strongly associated with the deprotonation/reduction of water molecules from the hydrated $[Zn(H_2O)_6]^{2+}$ ions (Fig. 1a).[3, 4] In aqueous electrolytes, it is particularly difficult to suppress these

undesired reactions, largely due to the inevitable generation of hydrated solvates and a hydrophilic anode-electrolyte interface.

Ideally, a hydrophobic anode-electrolyte interface with preferential exclusion of water from the interface would effectively minimize the footprint of water and its subsequent decomposition, thus enhancing the reversibility and lifespan of Zn^0 anodes. Current efforts for excluding water from the anode surface have primarily focused on wrapping the Zn^0 anode surface with either a naturally-formed solid-electrolyte interphase (SEI) layer that is typically derived from solvents and solutes,[5, 6] or artificial hydrophobic coatings[7-11]. However, the unsatisfactory compactness, strength, flexibility, and ionic conductivity of those native SEIs remain problematic, resulting in poor Zn plating/stripping efficiency and high polarization under high current densities. The wide application of artificial surface coatings would be limited by their fabrication complexity and lack of self-healing functionality that compromises the cycling durability. Directly leveraging organic electrolytes could completely remove water solvents and ideally eliminate the generation of hydrated solvates to offer a water-free anode-electrolyte interface, yet such electrolytes could suffer from the aforementioned combustion risks common to lithium-ion batteries.[12]

To simultaneously reduce the prevalence of interfacial side reactions and maintain fast reaction kinetics in aqueous electrolytes, one needs to maximize water exclusion from anode surface without introducing undesired SEI layers, which could be realized by introducing hydrophobicity into water-based electrolytes directly through the addition of functionalized molecules. In traditional hybrid electrolyte design, the added molecules either interact with both cations and anions by functioning as co-solvents[13, 14] or show negligible participation in the solvation process to work as "non-solvation diluents" that have been widely used to formulate localized high concentration electrolytes for lithium/sodium batteries.[15, 16] A water-rich (hydrophilic) layer on the

surface of Zn anodes is generally observed in these electrolytes. The possibility of forming localized hydrophobicity in either solvates/solvate clusters or directly on the Zn metal anode surface however has not been discussed in this context, because hydrophobicity is counterintuitive for any water-based systems.

In this work, we show that the "hydrophobic aqueous electrolyte" concept can be realized locally by introducing a "non-traditional" diluent with cation-philic and strongly anion-phobic properties. In this new solvation structure, the diluent molecule preferentially binds to the zinc cation (cation-philic), loses water bonding capability (hydrophobic), and repels the anion (anion-phobic), which not only depolarizes cation-shuttled waters but also allows the hydrophilic solvation region to be encapsulated inside a hydrophobic outer shell. Fulfilling "non-traditional" diluent criteria, dimethylformamide (DMF) was identified as the diluent for the baseline aqueous zinc sulfate ($ZnSO_4$) electrolyte. Since Zn^0 prefers DMF monomers over water monomers on its surface, free water would be largely excluded away from Zn^0 surface. The minimized footprint and weakened activity of water molecules on Zn^0 surface reduce the side reactions that involve water. More interestingly, DMF molecules can react with hydroxyl-ions without introducing undesired SEI layers, which further minimizes surface passivation and enables a smooth Zn plating morphology, whereby highly reversible Zn^0 deposition is supported even under high current density operations.

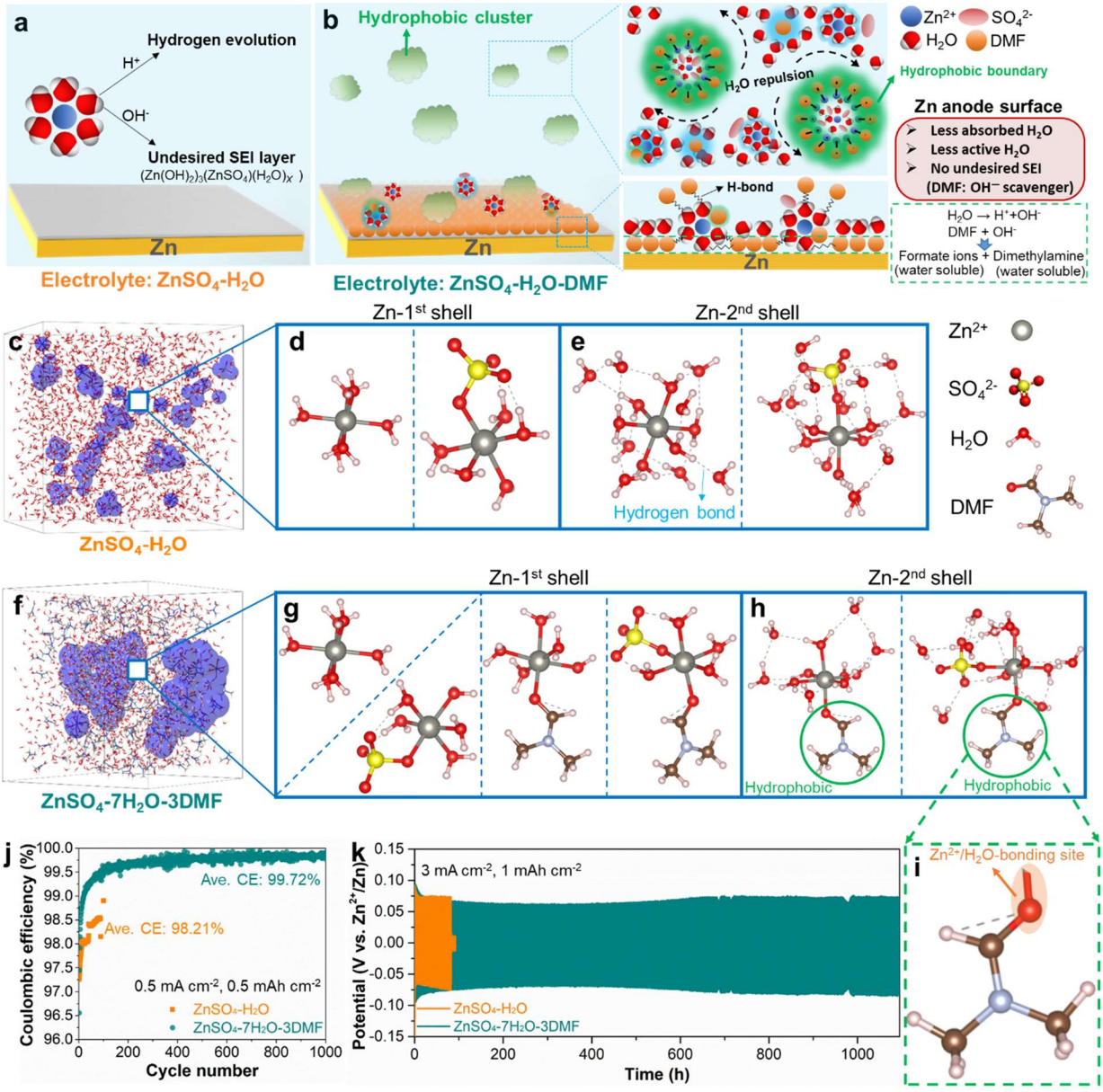

Figure 1. Calculated solvation structure of $ZnSO_4$-H_2O and $ZnSO_4$-$7H_2O$-3DMF and corresponding electrochemical performance of Zn^0 anodes in these two electrolytes. (a, b) Schematic illustration of solvent structure in bulk electrolyte and on the Zn^0 surface in (a) baseline $ZnSO_4$-H_2O and (b) hybrid $ZnSO_4$-H_2O-DMF. (c) Snapshot from the MD simulation for the $ZnSO_4$-H_2O with representative Zn^{2+}-solvation structures for the first shell (d) and partial second shells (e) in the $ZnSO_4$-H_2O. (f) Snapshot from the MD simulation for the $ZnSO_4$-$7H_2O$-3DMF with representative Zn^{2+}-solvation structures for the first shell, where blue isosurfaces show Zn^{2+} solvate distribution (g) and partial second shells (h) in the $ZnSO_4$-$7H_2O$-3DMF electrolyte. (i)

Representative coordination of DMF in the Zn^{2+}-solvation structure. (j) Coulombic efficiency of Zn plating/stripping in asymmetric Zn//Cu cells under different electrolytes. The cycling current density was 0.5 mA cm^{-2} and the cycling capacity was 0.5 mAh cm^{-2}. (K) Voltage-time profiles of Zn metal anodes in different electrolytes with a cycling capacity of 1 mAh cm^{-2} at 3 mA cm^{-2}.

Aqueous $ZnSO_4$ electrolyte (0.5 mol L^{-1}) was selected as the baseline (denoted as $ZnSO_4$-H_2O, Table S1) to validate our "hydrophobic aqueous electrolyte" concept, owing to its low cost (Table S2) and mild acidity. DMF with one polar group per molecule unit (acyl group, N-C=O, Fig. S1) was thereafter selected as the anion-phobic diluent of $ZnSO_4$ (denoted as $ZnSO_4$-H_2O-DMF hereafter), due to its strong affinity for Zn metal[12], its low freezing point (-64ºC), as well as its chemical reactivity with hydroxyl ions[17] that suppresses the basic salt precipitation on Zn^0 surface. In addition, DMF has a strong affinity for Zn^{2+} ions as it effectively dissolves many Zn salts including zinc perchlorate ($Zn(ClO_4)_2$), zinc bis(trifluoromethanesulfonyl)imide ($Zn(TFSI)_2$), and zinc trifluoromethane sulfonate ($Zn(OTf)_2$), *etc.*;[12, 18, 19] in these systems, DMF is a solvent/co-solvent of adopted zinc salts. However, DMF does not dissolve $ZnSO_4$ because of its low affinity for SO_4^{2-} anions.[20] More importantly, the Zn^{2+}-bonding (cation-philic) site in the DMF molecule is also the water-bonding (hydrogen-bonding and hydrophilic) site. Thus, the DMF molecules will transform from hydrophilic into hydrophobic molecules upon solvating Zn^{2+} ions, forming a hydrophobic layer at the boundary of the hydrophilic cluster (Fig. 1b). $ZnSO_4$-7H_2O-3DMF (H_2O/DMF volume ratio: 7/3) was selected as the main formulation of hybrid electrolytes for systematic investigations due to its well-balanced properties that include salt solubility (Fig. S2), ionic conductivity and viscosity (Fig. S3, Table S3 and S4), and electrochemical performance (Fig. S4). We found that $ZnSO_4$-7H_2O-3DMF displayed a freezing point of ~40 °C (Fig. S5) and could practically work at -30 °C with an ionic conductivity of 0.9 mS cm^{-1} (Fig. S6). In addition, such

hybrid electrolytes showed excellent fire-retardant capability even under a high H_2O/DMF ratio of 5:5 (Fig. S7).

According to MD simulations, in $ZnSO_4$-H_2O, Zn^{2+} was found to coordinate on average with 5.91 water molecules and 0.09 SO_4^{2-} anions in the primary solvation shells, consistent with the typical hexahydrate structure (i.e., $Zn[H_2O]_6^{2+}$) of non-concentrated, aqueous zinc electrolytes.[21, 22] Zinc species are uniformly distributed throughout the system as highlighted by the scattered blue regions (each centering on a Zn^{2+} in Fig. 1c and Fig. S8). Representative Zn^{2+}-solvation structures with first shells and partial second shells are displayed in Fig. 1d and 1e, respectively. In $ZnSO_4$-$7H_2O$-3DMF electrolyte, complexation with DMF molecules was observed in the first Zn^{2+}-solvation shell due to the strong affinity between DMF and Zn^{2+}, forming an average structure of $Zn^{2+}[H_2O]_{5.53}[DMF]_{0.25}[SO_4^{2-}]_{0.22}$. Interestingly, the Zn^{2+}-species tend to form water-rich and DMF-free nano-domains highlighted by blue isosurfaces (Fig. 1f and Fig. S9). There is a DMF-enriched phase with lesser amounts of free H_2O at the boundary of these domains. This unique structure possibly reflects an asymmetry in the solvating behavior of DMF and water for SO_4^{2-} and Zn^{2+} due to the inability of DMF to form hydrogen bonds with SO_4^{2-} in contrast to water (Note S1). $ZnSO_4$ species in these water-rich domains tend to remain solvent separated with only a minor increase in the formation of contact ion pairs (CIP). Cations near the DMF-enriched boundary were observed to exchange water/DMF (Fig. 1f-i). Aside from the hydrogen bonding between free DMF and free water, free DMF can also hydrogen bond to dangling OH groups from the coordinated H_2O in Zn^{2+} solvation shells through the carbonyl oxygen of DMF. However, after coordinating the hydrophilic carbonyl end of the molecule, the Zn^{2+}-coordinated DMF clusters become locally hydrophobic thanks to the dangling methyl groups, and repel free water molecules away, thus favoring to form a hydrophobic anode-electrolyte interface when the DMF-involved

Zn^{2+} solvates (or solvate clusters) approach the Zn anode during the Zn plating process (Fig. 1b). Note that despite DMF has been introduced into aqueous Zn electrolytes,[19] the localized hydrophobicity formation possibility has never been predicted or discussed before.

Owing to the unique solvation structures of hybrid electrolytes, the Zn metal batteries delivered high reversibility and long lifetime in $ZnSO_4$-$7H_2O$-3DMF. For instance, the Zn//Cu cells in $ZnSO_4$-$7H_2O$-3DMF showed a high average CE of ~99.72% at 0.5 mA cm^{-2} (Fig. 1j) and ~99.81% at 1 mA cm^{-2} (Fig. S10). In contrast, an average CE of only 98.21% and 98.76% was achieved for the Zn//Cu cells (before failure) in $ZnSO_4$-H_2O at 0.5 mA cm^{-2} and 1 mA cm^{-2}, respectively (Fig. 1j and Fig. S10). Even under a strict CE evaluation protocol,[23] the Zn//Cu cell in $ZnSO_4$-$7H_2O$-3DMF demonstrated a higher CE than that using $ZnSO_4$-H_2O (98.5% vs. 94.8%, Fig. S11). Furthermore, the symmetric Zn//Zn cells using the $ZnSO_4$-$7H_2O$-3DMF presented stable polarization with a greatly extended lifetime, e.g., over 2950 h at 0.2 mA cm^{-2}, 0.2 mAh cm^{-2}, and 1100 h at 3 mA cm^{-2}, 1 mAh cm^{-2} (Fig. 1k and Fig. S12). However, the Zn//Zn cells in the baseline $ZnSO_4$-H_2O were generally shorted after limited cycles (Fig. 1k and Fig. S12). A maximal cumulative plating capacity of 1650 mAh cm^{-2} is realized in $ZnSO_4$-$7H_2O$-3DMF at 3 mA cm^{-2}, which is superior to a number of reported Zn//Zn symmetric cells using aqueous and non-aqueous electrolytes (Fig. S13 and Table S5).

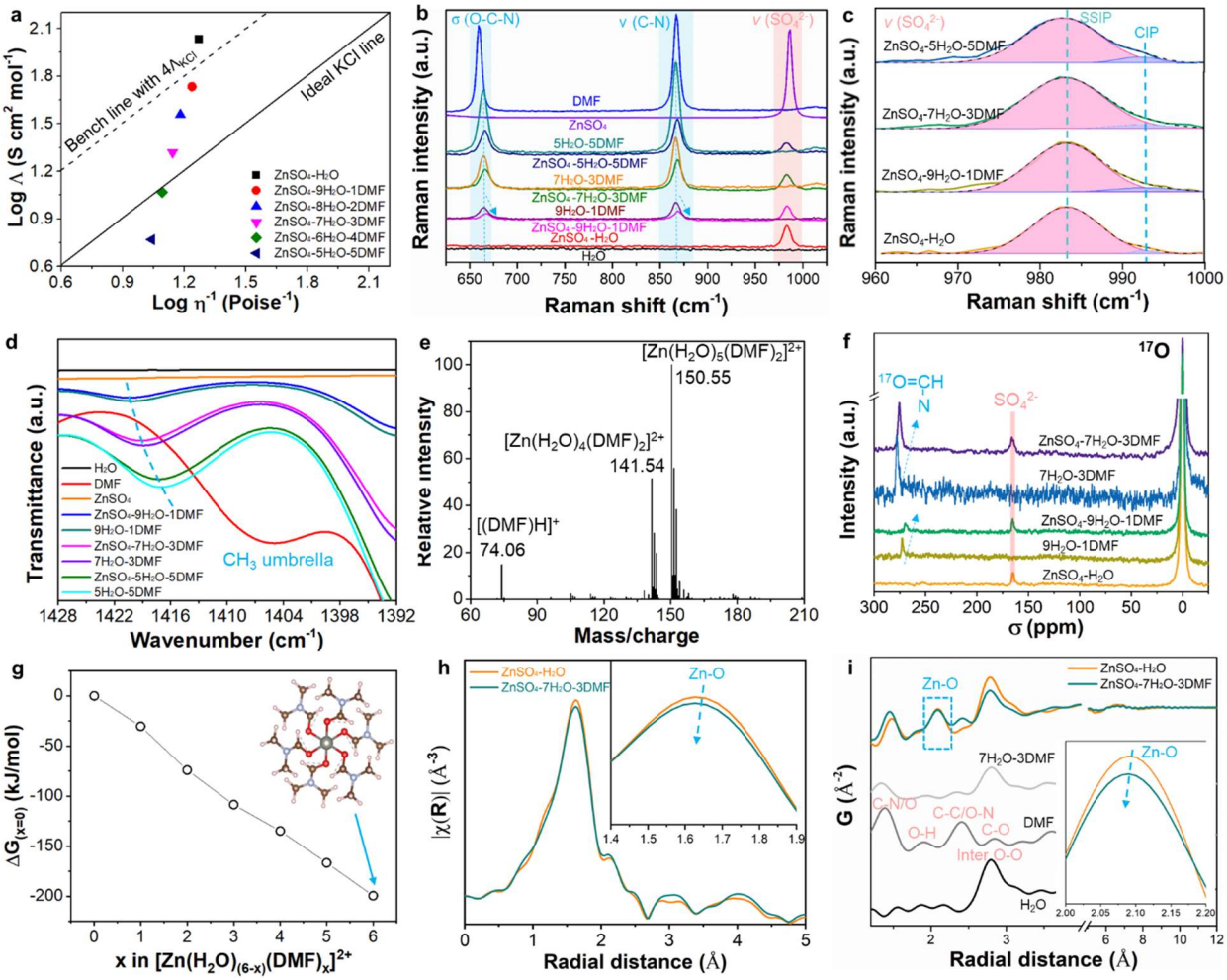

Figure 2. Elucidating the structure of $ZnSO_4$-H_2O and $ZnSO_4$-H_2O-DMF. (a) Walden plot showing relationships between inverse viscosity and molar conductivity for $ZnSO_4$−H_2O and $ZnSO_4$−H_2O-DMF. (b) Raman spectra of neat H_2O, DMF solvents, H_2O/DMF mixture, baseline $ZnSO_4$−H_2O, and hybrid $ZnSO_4$−H_2O-DMF with different H_2O/DMF volume ratios. (c) Raman spectra showing the SO_4^{2-} anion vibration in different electrolytes. (d) ATR-FTIR spectra of the solvents, baseline electrolyte and hybrid electrolytes. (e) Ionic high resolution mass spectra (HR-MS) of $ZnSO_4$−$7H_2O$-3DMF in the positive-ion mode. (f) ^{17}O NMR spectra for H_2O/DMF mixture, $ZnSO_4$−H_2O, $ZnSO_4$−H_2O-DMF with different H_2O/DMF volume ratios. (g) Relative binding free energies of Zn^{2+} solvation shell from PCM(=20)/M052X/6-311++G (2df, 2pd) from the hexahydrate to the hexa-coordinated $Zn(DMF)_6$ cluster. It should be noted that DMF is not expected to replace all six waters in Zn solvation shells, as a strong electrostatic interaction between Zn^{2+} and SO_4^{2-} can be observed even in SSIP, which retards the coordination of DMF-Zn^{2+}. (h)

Fourier transformed extended X-ray absorption fine structure (ftEXAFS) spectra of the $ZnSO_4$−H_2O and $ZnSO_4$−$7H_2O$-3DMF. The inset in (h) shows the magnified area of the Zn-O bond. (i) X-ray pair distribution function (PDF) of H_2O, DMF, H_2O/DMF mixture, $ZnSO_4$−H_2O, and $ZnSO_4$−$7H_2O$-3DMF. The inset in (i) shows the magnified X-ray PDF of Zn-O bond for the $ZnSO_4$−H_2O and $ZnSO_4$−$7H_2O$-3DMF.

Walden plots show that the non-concentrated aqueous electrolyte (0.5M $ZnSO_4$−H_2O) is slightly above the bench line with a 4-fold conductivity of ideal KCl solution (dash line in Fig. 2a), indicating the ions in the electrolyte are mostly dissociated and the interionic interactions are weak.[24, 25] A factor of four accounts for the charge squared term in the Nernst – Einstein expression relating conductivity to ion diffusion. In comparison, the hybrid 0.5M $ZnSO_4$−H_2O-DMF electrolytes all fall below the bench line, attributed to a slight increase of salt association and increased size of the Zn solvation shell upon the addition of "bulky" DMF (*vs*. H_2O) that prevent independent motion of the ions in the electrolytes. Raman peak shift of characteristic O-C-N scissor mode (σ(O-C-N), at around 665 cm^{-1}) and C-N stretching mode (ν(C-N), at around 868 cm^{-1})[26] upon the addition of $ZnSO_4$ into the DMF/H_2O mixture (Fig. 2b) suggests the interaction between Zn^{2+} and DMF, which was further confirmed by the blue shift of CH_3 umbrella mode[27] between Zn^{2+}-free DMF/H_2O mixtures and Zn^{2+}-containing DMF/H_2O mixtures in the ATR-FTIR spectra (Fig. 2d). The strong hydrogen bonding between DMF and H_2O can be demonstrated by the characteristic peak shift of pure DMF after the addition of H_2O in the Raman spectra (Fig. S14) and the ATR-FTIR spectra (Fig. 2d and Fig. S15), where the DMF/H_2O interaction helps to break the hydrogen bonding network among free water molecules and suppresses HER.[13, 28, 29] Meanwhile, the quantitative fitting of SO_4^{2-} resonance showed that the CIP fraction slightly increased with DMF contents in the hybrid electrolyte (Fig. 2c and Table S6), consistent with the

Walden plots analysis and the molecule dynamics (MD) result. This phenomenon is different from the dramatically elevated content ratio of CIP over SSIP (solvent separated ion pair) when increasing the concentration of solute[8] or increasing the content of co-solvents that have a strong affinity for both cations and anions.[22]

The involvement of DMF in the Zn^{2+}-solvation sheaths was evidenced by high-resolution mass spectrometry (HRMS) of $ZnSO_4$-7H_2O-3DMF in the positive-ion mode, where the signals of DMF-containing $[Zn(H_2O)_4(DMF)_2]^{2+}$ and $[Zn(H_2O)_5(DMF)_2]^{2+}$ complexes can be detected (Fig. 2e). Furthermore, there is no signal for any SO_4^{2-} species solvated by DMF molecules in the HRMS spectrum of $ZnSO_4$-7H_2O-3DMF in the negative-ion mode (Fig. S16), similar to that of $ZnSO_4$-H_2O (Fig. S17), implying that DMF has a low affinity for SO_4^{2-} anions. Above observations are also consistent with the previous report of $CuSO_4$ in H_2O/DMF.[20] The interaction between Zn^{2+} and DMF, particularly the lone-pair electrons on O from DMF, was convincingly confirmed by the upfield shift (with a lower σ) of both ^1H and ^{17}O from DMF upon dissolution of $ZnSO_4$ in neat DMF/H_2O mixtures (Fig. 2f and Fig. S18). In contrast, the chemical shift of ^{17}O from SO_4^{2-} anions remained unchanged before and after introducing DMF into the $ZnSO_4$-H_2O baseline, implying that the DMF has negligible interaction with SO_4^{2-} anions. The cation-philic and anion-phobic property of DMF toward $ZnSO_4$ was further validated by the experimental observation that DMF can dissolve $Zn(OTf)_2$ salt but showed poor solubility to most of the sulfates (Fig. S19 and S20). Furthermore, DFT calculations show a nearly linear decrease in the binding free energy upon the incremental replacement of H_2O for DMF in the Zn^{2+} solvation shell (Fig. 2g), demonstrating that DMF is thermodynamically favorable to coordinate with Zn^{2+} ions. This result is in line with higher reorganization energy of $Zn^{2+}(DFM)(H_2O)_5$ than $Zn^{2+}(H_2O)_6$ during desolvation (Table S8 and

Note S2), as well as the higher activation energy of Zn^{2+} conduction and Zn^{2+} transfer in $ZnSO_4$-$7H_2O$-3DMF than in $ZnSO_4$-H_2O (Fig. S21).

The strong interaction couple of Zn^{2+}-DMF would weaken the binding between Zn^{2+} and H_2O, which was evidenced by the X-ray absorption spectroscopy (XAS) and X-ray pair distribution function (PDF) analysis. The Zn XANES spectra manifest that the Zn edge position in the $ZnSO_4$-$7H_2O$-3DMF shifts to the lower energy direction compared with the case in the $ZnSO_4$-H_2O (Fig. S22). This implies that the electron transfer between Zn and O (from H_2O or DMF) is reduced upon the addition of DMF, thus weakening the bonding strength between Zn^{2+} and H_2O in the solvation structure.[6] Both the ft-EXAFS (Fig. 2h) and PDF spectra (Fig. 2i) verify that the average bond length of Zn-O is slightly smaller in $ZnSO_4$-$7H_2O$-3DMF than that in $ZnSO_4$-H_2O, which was attributed to the strong bonding between DMF and Zn^{2+}. This conclusion is also consistent with radial distribution functions (RDFs) obtained by MD simulations (Fig. S23).

X-ray diffraction (XRD) patterns unveil that much more byproduct of ZHS ($Zn_4(OH)_6(SO_4)\cdot 5H_2O$) could be identified on the Zn electrode when cycled in the baseline $ZnSO_4$-H_2O than those in the hybrid $ZnSO_4$-H_2O-DMF (Fig. 3a-b), and the byproduct signal nearly vanished for the H_2O:DMF volume ratios of 7:3 and 6:4. The suppressed passivation in $ZnSO_4$-H_2O-DMF electrolytes was also verified by X-ray photoelectron spectroscopy (XPS) analysis (Fig. S24), electrochemical impedance spectrum (EIS) test (Fig. S25), and TEM characterization (Fig. S26-28). TEM characterizations also confirmed that there is no typical SEI film formation on Zn^0 surface cycled in neither $ZnSO_4$-H_2O nor $ZnSO_4$-$7H_2O$-3DMF. Here, the absence of DMF-derived SEI layer is probably due to the inherent water-solubility of DMF-originated decomposed species, including dimethylamine and formate ions (Fig. 1b).[17] The suppressed byproduct formation in $ZnSO_4$-H_2O-DMF is owing to following aspects: (1) Suppressed water reduction and OH^-

generation due to the less active water (released from Zn^{2+}-solvation sheath) and less absorbed free water on Zn^0 surface in hybrid electrolytes, in which DMF molecules have better Zn^0 wettability (higher zincophilicity) than water molecules (Fig. S29) and DMF rather than water molecules would preferentially bond with Zn^0 surface through the polar acyl groups (N-C=O)[12, 30] even though DMF does not facilitate Zn^{2+} desolvation kinetics (Fig. S30 and Note S1). (2) DMF molecules on Zn^0 anode surface can further react with OH^- if locally generated by water reduction,[17] thus minimizing the ZHS formation (see schematic in Fig. 1b). (3) Suppressed water reduction leads to less proton loss, which mitigates the pH increase and ZHS formation.[31-33]

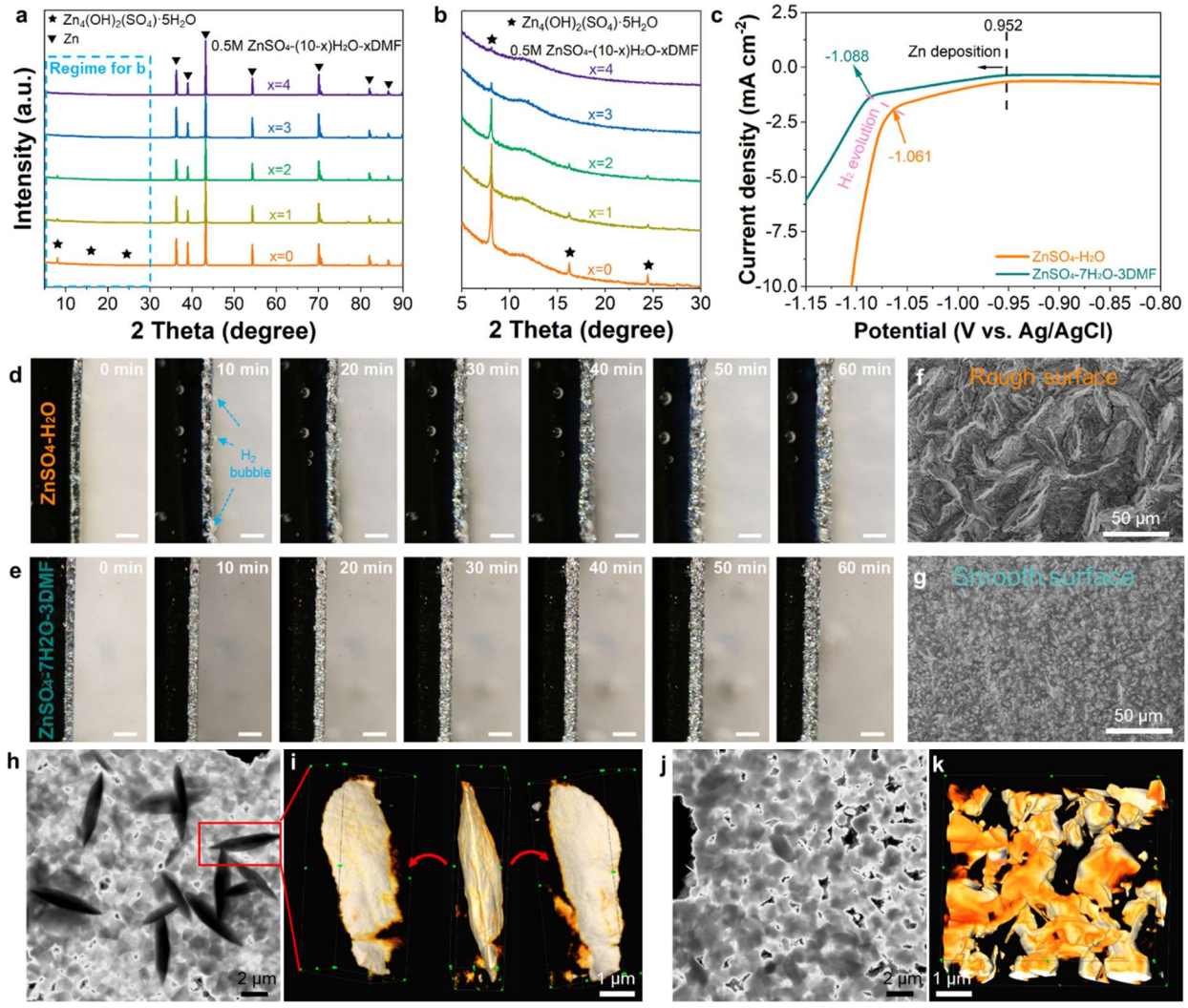

Figure 3. Passivation and corrosion behaviors on the Zn^0 surface in $ZnSO_4$-H_2O and $ZnSO_4$-H_2O-DMF. (a) XRD patterns of Zn electrodes after cycling in Zn//Cu cells at 1 mA cm^{-2} with the cycling capacity of 1 mAh cm^{-2} for 100 cycles. (b) XRD patterns showing the formation of $Zn_4(OH)_6(SO_4)\cdot 5H_2O$ byproduct on the surface of cycled Zn electrodes, which are zoomed from (a). (c) Linear sweep voltammetry (LSV) analysis on the HER properties of $ZnSO_4$−H_2O and $ZnSO_4$-$7H_2O$-3DMF. (d, e) In-situ optical observations of Zn^0 plating in (d) $ZnSO_4$−H_2O and (e) $ZnSO_4$-$7H_2O$-3DMF, where H_2 bubbles can be well identified in $ZnSO_4$−H_2O. The testing current density was 10 mA cm^{-2}. Scale bars in (d, e) are 200 μm. (f, g) SEM images of the Zn electrodes after testing in (f) $ZnSO_4$−H_2O and (g) $ZnSO_4$-$7H_2O$-3DMF. (h-k) scanning transmission electron microscopy image and reconstructed 3D electron tomogram of incipient stage Zn^0 plating in the (h, i) $ZnSO_4$−H_2O and (j, k) $ZnSO_4$-$7H_2O$-3DMF, where the plating current was 3 mA cm^{-2} and the plating time was 10 min.

Linear sweep voltammetry (LSV) test (Fig. 3c) and linear polarization experiments (Fig. S31) showed a delayed H_2 evolution potential and lower corrosion rate in $ZnSO_4$-$7H_2O$-3DMF than $ZnSO_4$-H_2O, which is consistent with the DFT result that HER potential reduces with introduction of DMF and/or sulfate into the solvation shell (voltages vs Zn^{2+}/Zn): -0.26 V $ZnSO_4(DMF)(H_2O)_4$ < -0.11 V $ZnSO_4(H_2O)_5$ < 0.14 V $Zn(DMF)(H_2O)_5$ < 0.30 V $Zn(H_2O)_6$. The H_2 evolution behavior was also visualized by in-situ optical microscope observations, in which massive H_2 bubbles were identified on Zn^0 in $ZnSO_4$-H_2O (Fig. 3d and Movie S1) while no visible H_2 bubbles were found in $ZnSO_4$-$7H_2O$-3DMF (Fig. 3e and Movie S2). Furthermore, Zn^0 showed a rough surface after 60 min plating in $ZnSO_4$-H_2O (Fig. 3f); in contrast, smooth Zn^0 plating was observed in $ZnSO_4$-$7H_2O$-3DMF (Fig. 3g). In addition, scanning transmission electron microscopy and electron tomography reveal in the baseline aqueous electrolyte, at the very early stage of Zn^0 plating, blade-shaped dendrite precursors form on a conformally plated Zn^0 layer (Fig. 3h and 3i). On the other hand, in

the $ZnSO_4$-$7H_2O$-3DMF electrolyte, the dendrite precursors are completely eliminated (Fig. 3j and 3k).

Aside from regulating solvation structure, the adoption of an anion-phobic diluent can also impact the Zn^0 nucleation kinetics and surface morphology. As shown in Fig. 4a-b, Fig. S32 and S33, Zn^0 in $ZnSO_4$-$7H_2O$-3DMF displayed a shorter 2D nucleation/growth time than those in $ZnSO_4$-H_2O under various testing potentials from 30 mV to 150 mV, implying the Zn^0 nucleation/growth in $ZnSO_4$-$7H_2O$-3DMF would be more homogeneous (Fig. 4c).[10, 34] The random/irregular Zn^0 nucleation/growth pattern in $ZnSO_4$-H_2O and smooth Zn^0 nucleation/growth pattern in $ZnSO_4$-$7H_2O$-3DMF were revealed by ex-situ SEM measurements (Fig. 4d-e and Fig. S33) and digital images of Zn^0 foils after test (Fig. 4f). The favorable Zn^0 deposition behavior in $ZnSO_4$-H_2O-DMF was further confirmed by the lower nucleation overpotential and lower plating overpotential of Zn//Cu cell at 0.05 mA cm^{-2} (Fig. 4g). In addition, the polarization became smaller with increasing DMF content (Table S7), implying that DMF promotes Zn^0 plating when mass transfer influence is excluded. Even after long-term cycling at 1 mA cm^{-2} for 100 cycles in Zn//Cu cells, the cycled Zn electrode and Cu electrode in $ZnSO_4$-H_2O-DMF showed much smoother morphology than those in baseline $ZnSO_4$-H_2O (Fig S34 and S35).

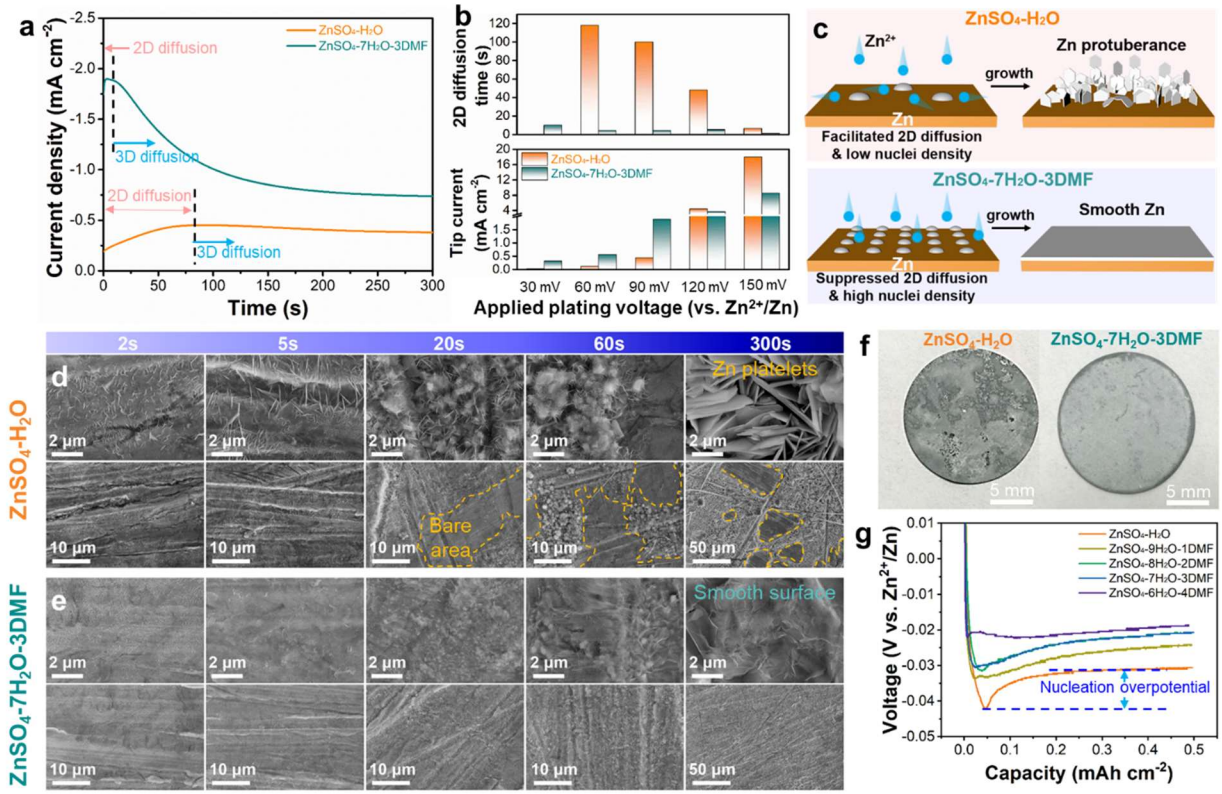

Figure 4. Zn^0 nucleation kinetics and morphology evolution in $ZnSO_4$-H_2O and $ZnSO_4$-H_2O-DMF. (a) Current-time profiles of Zn^0 nucleation on Zn^0 foils in different electrolytes at the applied potential of 90 mV (vs Zn^{2+}/Zn). (b) Comparison of (upper) 2D diffusion time and (lower) tip current of Zn^0 nucleation on Zn^0 foils in different electrolytes with a series of applied potentials. (c) Schematic illustration of the nucleation process in (upper) $ZnSO_4$-H_2O and (lower) $ZnSO_4$-$7H_2O$-3DMF. (D, E) SEM images of Zn electrodes after Zn plating for 2s, 5s, 20s, 60s, and 300s at the applied voltage of 150 mV in (d) $ZnSO_4$-H_2O and (e) $ZnSO_4$-$7H_2O$-3DMF. (f) Digital images of Zn electrode after Zn plating for 300s at the applied voltage of 150 mV in (left) $ZnSO_4$–H_2O and (right) $ZnSO_4$-$7H_2O$-3DMF. (g). Voltage profiles for the initial Zn^0 nucleation at 0.05 mA cm^{-2} in baseline $ZnSO_4$-H_2O and a series of hybrid $ZnSO_4$-H_2O-DMF.

Owing to the extended temperature window of hybrid electrolytes, both Zn//Cu and Zn//Zn cells based on $ZnSO_4$-7H_2O-3DMF can stably operate at -10 °C (Fig. 5a and 5b). Meanwhile, $ZnSO_4$-H_2O freezes at -10 °C (inset in Fig. 5a), and the as-constructed cell cannot be initiated. The merits of $ZnSO_4$-7H_2O-3DMF were further verified in zinc ion capacitors (Zn//AC, AC: activated carbon) and zinc ion batteries (Zn//MnO_2) with limited Zn sources. At room temperature, the Zn//AC capacitor (N/P ratio, ~11:1) can stably operate for 5000 cycles with 80.6% capacity retention (Fig. 5c), while the Zn//MnO_2 battery (N/P ratio, ~4:1) maintained capacity retention of 50.4% after 2000 cycles at 5C (Fig. S36). Conversely, both the zinc ion capacitor and zinc ion battery using the baseline electrolyte showed a rapid capacity decay with a final dendrite-induced short circuit. In addition, the $ZnSO_4$-7H_2O-3DMF electrolyte also supported the stable operation of Zn//AC capacitors at -10 °C (Fig. 5d). The locally hydrophobic structure created by the cation-philic, anion-phobic, and OH^--reactive diluent (DMF) is also effective for other electrolyte systems containing zinc acetate ($Zn(Ac)_2$) solute. Enhanced CE and lifetime along with limited byproducts formation have been verified for Zn^0 anodes in $Zn(Ac)_2$–7H_2O-3DMF, in comparison with their baseline counterparts (Fig. 5e, 5f and Fig. S37), thus proving the generalizability of the hydroxyl ion-scavenging and localized hydrophobicity approach.

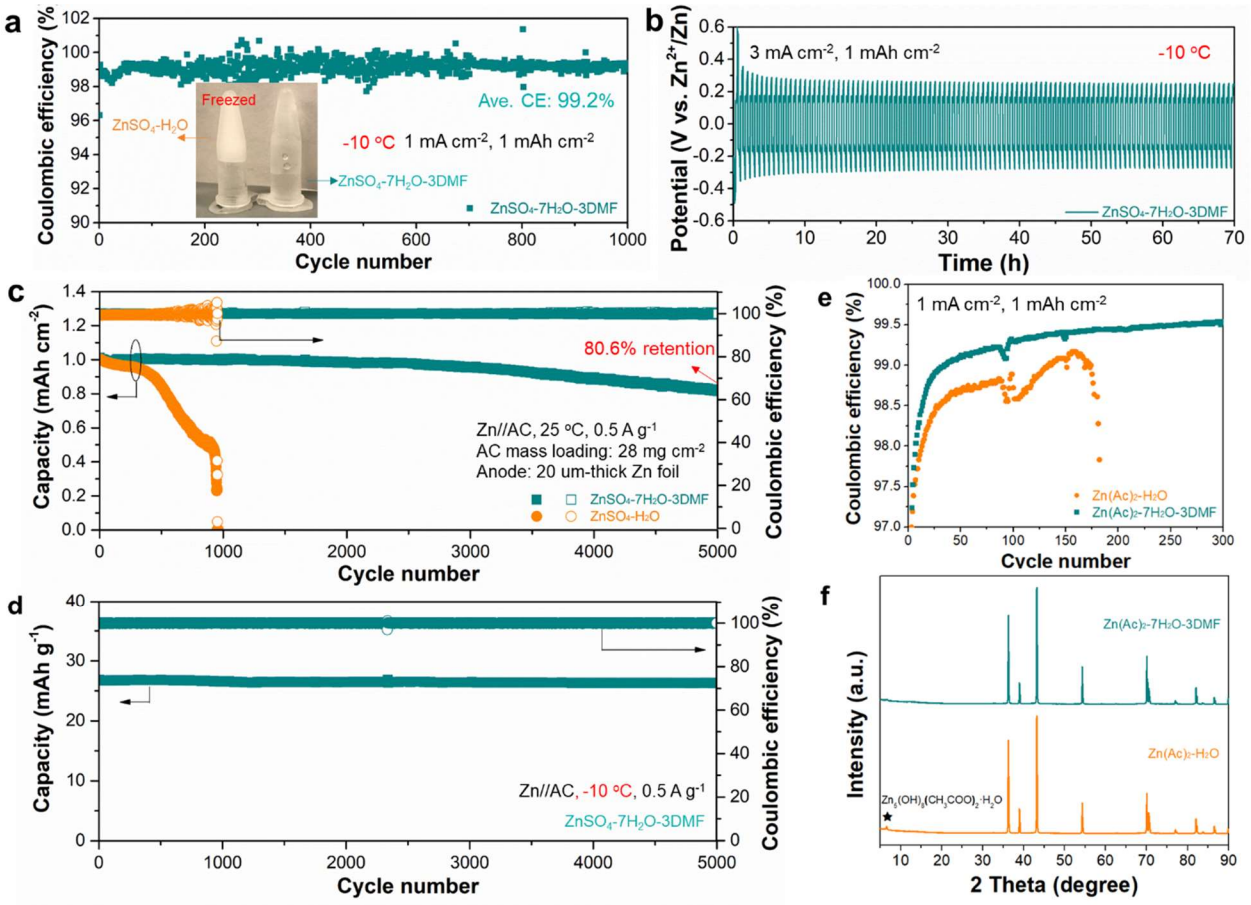

Figure 5. Versatility of the "hydrophobic aqueous electrolyte". (a) Coulombic efficiency of Zn plating/stripping on Cu foils using the Zn/Cu configuration in $ZnSO_4$-$7H_2O$-3DMF electrolyte under -10 °C with a cycling capacity of 1 mAh cm^{-2} at 1 mA cm^{-2}. (b) Voltage-time profiles of Zn metal anodes in $ZnSO_4$-$7H_2O$-3DMF electrolyte under the condition of -10 °C with a cycling capacity of 1 mAh cm^{-2} at 3 mA cm^{-2}. (c, d) Long-term cycling performance of Zn//AC capacitor at 0.5 A g^{-1} using $ZnSO_4$–H_2O and $ZnSO_4$-$7H_2O$-3DMF electrolytes at (c) 25 °C and (d) -10 °C. The mass loading of AC tested at -10 °C is 5 mg cm^{-2}. (e) Coulombic efficiency of Zn plating/stripping on Cu foils using the Zn//Cu configuration in $Zn(Ac)_2$-H_2O and $Zn(Ac)_2$-$7H_2O$-3DMF. (f) XRD patterns showing the formation of basic zinc acetate ($Zn_5(OH)_8(CH_3COO)_2 \cdot 2H_2O$) byproduct on the surface of cycled Zn electrodes (from Zn//Cu cells) in $Zn(Ac)_2$-H_2O and $Zn(Ac)_2$-$7H_2O$-3DMF after 100 cycles with a cycling capacity of 1 mAh cm^{-2} at 1 mA cm^{-2}.

In summary, we report a "hydrophobic aqueous electrolyte" with hydroxyl-ion scavenging functionality for aqueous Zn batteries, in which salt and water-enriched regions are encapsulated by a hydrophobic layer due to partial substitution of a cation-philic but anion-phobic diluent into the solvation shell of Zn^{2+} in solution. The resulting electrolyte induces less/weakened water and free alkalinity at the electrolyte-Zn^0 interface, leading to suppressed water reduction, minimization of unwanted passivation, and enhanced Zn^0 reversibility. The localized hydrophobicity and hydroxyl-ion-scavenging concept could provide a general approach to improve aqueous electrolytes for a host of emerging aqueous metal battery chemistries, all of which suffer from irreversible reactions of metal and water. The proposed "non-traditional diluent" with asymmetric cation/anion solvating characteristics is distinct among conventional diluents and co-solvents, which could also inspire more new electrolyte designs for non-aqueous batteries.

ASSOCIATED CONTENT

Supporting Information.

Supporting information includes electrolyte preparation; electrode preparation; methods; simulations; ionic conductivity; viscosity; working temperature window; solvation structure; CE; long-term polarization; Raman spectra, ATR-FTIR spectra; HR-MS; ^{1}H NMR spectra; digital images of DMF-involved mixtures; activation energy of different electrolytes; XANES spectra; contact angle analysis; simulated adsorption energy of different species on Zn and ZnO; XPS spectra of cycled Zn anode; TEM images of cycled Zn anode; EIS; linear polarization curve; SEM images of Zn metal nucleation and Zn cycling in different electrolytes; long-term cycling of Zn//MnO_2 full cells; table of different Zn salts' price; table of electrolyte formulations; table of conductivity, viscosity and pH value for different electrolytes; table of electrochemical

performance comparison between this work and reported works; table of SSIP and CIP in different electrolytes; table of nucleation/plating overpotential comparison between different electrolytes; table of calculated interaction energy and relative binding energy; note of discussion about the solvation structure and "non-traditional diluent" behavior of DMF; note of discussion about the SO_4^{2-}-phobic property of DMF; note of discussion about the DMF influence on Zn^{2+} desolvation.

AUTHOR INFORMATION

Corresponding Author

***Email address: rulin@jpl.nasa.gov**

***Email address: conrad.k.xu.civ@army.mil**

***Email address: huolinx@uci.edu**

Author Contributions

P.Z. and R.L. contributed equally to this work. H.L.X., R.L., and K.X. conceived and designed the experiments. P.Z. and R.L. prepared the materials and performed the electrochemical experiments. T.P. and O.B. conducted the DFT calculations and MD simulations. R.L. C.W and H.L.X, performed the TEM experiments. E.H. conducted the PDF measurement. L.M. carried out the XAS experiment. All authors discussed and analyzed the data. P.Z., R.L., T.P., K.X., O.B., E.H., and H.L.X. wrote the original draft with review and editing from all authors.

ACKNOWLEDGMENT

We at the UCI acknowledge the support from the U.S. Department of Energy, under award no. DE-SC0021204 and the start-up funding of H.L.X from UCI. The authors acknowledge the use of facilities and instrumentation at the UC Irvine Materials Research Institute (IMRI), which is

supported in part by the National Science Foundation through the UC Irvine Materials Research Science and Engineering Center (DMR-2011967). XPS was performed using instrumentation funded in part by the National Science Foundation Major Research Instrumentation Program under grant no. CHE-1338173. R. Lin, E. Hu and X.-Q. Yang at Brookhaven National Laboratory (BNL) are supported by the Assistant Secretary for Energy Efficiency and Renewable Energy, Vehicle Technology Office of the U.S. Department of Energy through the Advanced Battery Materials Research (BMR) Program, under contract DE-SC0012704. T. Pollard, O. Borodin and K. Xu at ARL are supported by Joint Center of Energy Storage Research (JCESR), an energy hub funded by DOE Office of Science. This research used resources 28-ID-2 and 7-BM of the National Synchrotron Light Source II, a U.S. Department of Energy (DOE) Office of Science User Facility operated for the DOE Office of Science by Brookhaven National Laboratory under Contract No. DE-SC0012704.

REFERENCES

1. Zhang, N.; Chen, X.; Yu, M.; Niu, Z.; Cheng, F.; Chen, J. Materials chemistry for rechargeable zinc-ion batteries. *Chem. Soc. Rev.* **2020,** 49, 4203-4219.

2. Blanc, L. E.; Kundu, D.; Nazar, L. F. Scientific challenges for the implementation of Zn-ion batteries. *Joule* **2020,** 4, 771-799.

3. Sui, Y.; Ji, X. Anticatalytic strategies to suppress water electrolysis in aqueous batteries. *Chem. Rev.* **2021,** 121, 6654-6695.

4. Li, C.; Xie, X.; Liang, S.; Zhou, J. Issues and future perspective on zinc metal anode for rechargeable aqueous zinc-ion batteries. *Energy Environ. Mater.* **2020,** 3, 16-159.

5. Cao, L.; Li, D.; Pollard, T.; Deng, T.; Zhang, B.; Yang, C.; Chen, L.; Vatamanu, J.; Hu, E.; Hourwitz, M. J.; Ma, L.; Ding, M.; Li, Q.; Hou, S.; Gaskell, K.; Fourkas, J. T.; Yang, X. Q.; Xu, K.; Borodin, O.; Wang, C. Fluorinated interphase enables reversible aqueous zinc battery chemistries. *Nat. Nanotechnol.* **2021,** 16, 902-910.

6. Cao, L.; Li, D.; Hu, E.; Xu, J.; Deng, T.; Ma, L.; Wang, Y.; Yang, X. Q.; Wang, C. Solvation structure design for aqueous Zn metal batteries. *J. Am. Chem. Soc.* **2020,** 142, 21404-21409.

7. Cao, L.; Li, D.; Deng, T.; Li, Q.; Wang, C. Hydrophobic organic electrolyte protected Zn anodes for aqueous Zn batteries. *Angew. Chem. Int. Ed. Engl.* **2020,** 59, 19292-19296.

8. Yang, H.; Chang, Z.; Qiao, Y.; Deng, H.; Mu, X.; He, P.; Zhou, H. Constructing a super-saturated electrolyte front surface for stable rechargeable aqueous zinc batteries. *Angew. Chem. Int. Ed. Engl.* **2020,** 59, 9377-9381.

9. Cui, Y.; Zhao, Q.; Wu, X.; Chen, X.; Wang, Y.; Qin, R.; Ding, S.; Song, Y.; Wu, J.; Yang, K.; Wang, Z.; Mei, Z.; Song, Z.; Wu, H.; Jiang, Z.; Qian, G.; Yang, L.; Pan, F.; Yang, J. An interface bridged organic-inorganic layer suppressing dendrite and side reactions for ultra-long life aqueous Zn metal anodes. *Angew. Chem. Int. Ed.* **2020,** 132, 16737-16744.

10. Zhao, Z.; Zhao, J.; Hu, Z.; Li, J.; Li, J.; Zhang, Y.; Wang, C.; Cui, G. Long-life and deeply rechargeable aqueous Zn anodes enabled by a multifunctional brightener-inspired interphase. *Energy Environ. Sci.* **2019,** 12, 1938-1949.

11. Zou, P.; Nykypanchuk, D.; Doerk, G.; Xin, H. L. Hydrophobic molecule monolayer brush-tethered zinc anodes for aqueous zinc batteries. *ACS Appl. Mater. Interfaces* **2021,** 13, 60092–60098.

12. Wang, N.; Dong, X.; Wang, B.; Guo, Z.; Wang, Z.; Wang, R.; Qiu, X.; Wang, Y. Zinc-organic battery with a wide operation-temperature window from -70 to 150 °C. *Angew. Chem. Int. Ed. Engl.* **2020,** 132, 14685-14691.

13. Chang, N.; Li, T.; Li, R.; Wang, S.; Yin, Y.; Zhang, H.; Li, X. An Aqueous hybrid electrolyte for low-temperature zinc-based energy storage devices. *Energy Environ. Sci.* **2020,** 13, 3527-3535.

14. Shi, J.; Xia, K.; Liu, L.; Liu, C.; Zhang, Q.; Li, L.; Zhou, X.; Liang, J.; Tao, Z. Ultrahigh coulombic efficiency and long-life aqueous Zn anodes enabled by electrolyte additive of acetonitrile. *Electrochim. Acta* **2020,** 358, 136937.

15. Zhang, X.; Zou, L.; Xu, Y.; Cao, X.; Engelhard, M. H.; Matthews, B. E.; Zhong, L.; Wu, H.; Jia, H.; Ren, X.; Gao, P.; Chen, Z.; Qin, Y.; Kompella, C.; Arey, B. W.; Li, J.; Wang, D.;

Wang, C.; Zhang, J. G.; Xu, W. Advanced electrolytes for fast-charging high-voltage lithium-ion batteries in wide-temperature range. *Adv. Energy Mater.* **2020,** 10, 2000368.

16. Cao, X.; Jia, H.; Xu, W.; Zhang, J.-G. Localized high-concentration electrolytes for lithium batteries. *J. Electrochem. Soc.* **2021,** 168, 010522.

17. Buncel, E.; Symons, E. The inherent instability of dimethylformamide–water systems containing hydroxide ion. *J. Chem. Soc., Chem. commun.* **1970,** 1970, 164-165.

18. Asada, M.; Fujimori, T.; Fujii, K.; Kanzaki, R.; Umebayashi, Y.; Ishiguro, S.-i. Solvation structure of magnesium, zinc, and alkaline earth metal ions in N,N-dimethylformamide, N,N-dimethylacetamide, and their mixtures studied by means of Raman spectroscopy and DFT calculations—Ionic size and electronic effects on steric congestion. *J. Raman Spectrosc.* **2007,** 38, 417-426.

19. Ma, Y.; Zhang, Q.; Liu, L.; Li, Y.; Li, H.; Yan, Z.; Chen, J. N, N–dimethylformamide tailors solvent effect to boost Zn anode reversibility in aqueous electrolyte. *National Science Review* **2022,** nwac051.

20. Tsierkezos, N. G.; Roithova, J.; Schröder, D.; Molinou, I. E.; Schwarz, H. Solvation of copper (II) sulfate in binary water/N, N-dimethylformamide mixtures: From the solution to the gas phase. *J. Phys. Chem. B* **2008,** 112, 4365-4371.

21. Wang, F.; Borodin, O.; Gao, T.; Fan, X.; Sun, W.; Han, F.; Faraone, A.; Dura, J. A.; Xu, K.; Wang, C. Highly reversible zinc metal anode for aqueous batteries. *Nat. Mater.* **2018,** 17, 543-549.

22. Dong, Y.; Miao, L.; Ma, G.; Di, S.; Wang, Y.; Wang, L.; Xu, J.; Zhang, N. Non-concentrated aqueous electrolytes with organic solvent additives for stable zinc batteries. *Chem. Sci.* **2021,** 12, 5843-5852.

23. Ma, L.; Schroeder, M. A.; Borodin, O.; Pollard, T. P.; Ding, M. S.; Wang, C.; Xu, K. Realizing high zinc reversibility in rechargeable batteries. *Nat. Energy* **2020,** 5, 743-749.

24. Angell, C. A.; Byrne, N.; Belieres, J.-P. Parallel Developments in aprotic and protic ionic liquids: Physical chemistry and applications. *Acc. Chem. Res.* **2007,** 40, 1228-1236.

25. Angell, C. A.; Ansari, Y.; Zhao, Z. Ionic liquids: past, present and future. *Faraday Discuss.* **2012,** 154, 9-27.

26. Yang, B.; Lang, H.; Liu, Z.; Wang, S.; Men, Z.; Sun, C. Three stages of hydrogen bonding network in DMF-water binary solution. *J. Mol. Liq.* **2021,** 324, 114996.

27. Shastri, A.; Das, A. K.; Krishnakumar, S.; Singh, P. J.; Raja Sekhar, B. N. Spectroscopy of N,N-dimethylformamide in the VUV and IR regions: Experimental and computational studies. *J. Chem. Phys.* **2017,** 147, 224305.

28. Cui, J.; Liu, X.; Xie, Y.; Wu, K.; Wang, Y.; Liu, Y.; Zhang, J.; Yi, J.; Xia, Y. Improved electrochemical reversibility of Zn plating/stripping: a promising approach to suppress water-induced issues through the formation of H-bonding. *Mater. Today Energy* **2020,** 18, 100563.

29. Wang, Y.; Wang, T.; Dong, D.; Xie, J.; Guan, Y.; Huang, Y.; Fan, J.; Lu, Y.-C. Enabling high-energy-density aqueous batteries with hydrogen bond-anchored electrolytes. *Matter* **2022,** 5, 162-179.

30. Zhang, Q.; Luan, J.; Fu, L.; Wu, S.; Tang, Y.; Ji, X.; Wang, H. The three-dimensional dendrite-free zinc anode on a copper mesh with a zinc-oriented polyacrylamide electrolyte additive. *Angew. Chem. Int. Ed. Engl.* **2019,** 58, 15841-15847.

31. Mateos, M.; Harris, K. D.; Limoges, B.; Balland, V. Nanostructured electrode enabling fast and fully reversible MnO_2-to-Mn^{2+} conversion in mild buffered aqueous electrolytes. *ACS Appl. Energy Mater.* **2020,** 3, 7610-7618.

32. Fitz, O.; Bischoff, C.; Bauer, M.; Gentischer, H.; Birke, K. P.; Henning, H. M.; Biro, D. Electrolyte study with in operando pH tracking providing insight into the reaction mechanism of aqueous acidic Zn//MnO_2 batteries. *ChemElectroChem* **2021,** 8, 3553-3566.

33. Lee, B.; Seo, H. R.; Lee, H. R.; Yoon, C. S.; Kim, J. H.; Chung, K. Y.; Cho, B. W.; Oh, S. H. Critical role of pH evolution of electrolyte in the reaction mechanism for rechargeable zinc batteries. *ChemSusChem* **2016,** 9, 2948-2956.

34. Zou, P.; Zhang, R.; Yao, L.; Qin, J.; Kisslinger, K.; Zhuang, H.; Xin, H. L. Ultrahigh-rate and long-life zinc-metal anodes enabled by self-accelerated cation migration. *Adv. Energy Mater.* **2021,** 11, 2100982.

TOC

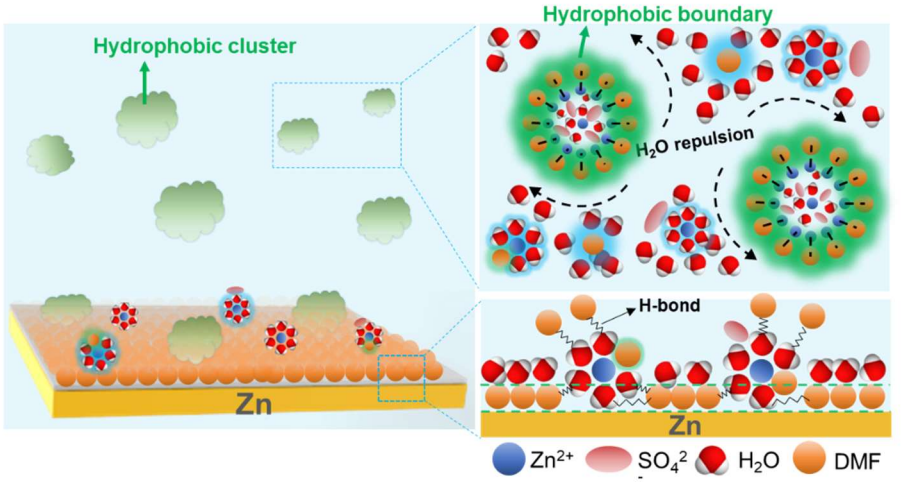

Localized hydrophobicity and interfacial alkalinity-scavenging in $ZnSO_4$-H_2O-DMF electrolyte